Journal of Natural Pesticide Research 1 (2022) 100003

Contents lists available at ScienceDirect

Journal of Natural Pesticide Research

journal homepage: www.journals.elsevier.com/journal-of-natural-pesticide-research

In silico-guided proposition of potential nematocidal and antibacterial *N*-(1,3,4-thiadiazol-2-yl)benzamides

Jessica S.F. Licona, Ingrid V. Pereira, Adriana C. de Faria, Joyce K. Daré, Elaine F.F. da Cunha, Matheus P. Freitas*

Department of Chemistry, Institute of Natural Sciences, Federal University of Lavras, 37200-900 Lavras, MG, Brazil

ARTICLE INFO

Keywords:
QSAR
Docking
Molecular modeling
Nematode
Rice bacteria

ABSTRACT

A series of amide derivatives containing the 1,3,4-thiadiazole moiety has been recently synthesized and tested against *Meloidogyne incognita* (Kofold & White) Chitwood (nematode) and *Xanthomonas oryzae* pv. *oryzae* (Ishiyama) Swings, van den Mooter, Vauterin, Hoste, Gillis, Mew & Kersters (rice bacteria). We have now reported the quantitative structure-activity relationship (QSAR) modeling of these biological activities, as well as docking studies to understand the action mechanisms of these compounds. Novel agrochemical candidates were proposed based on an interplay of the substituents which most affect the biological data. The reliable and predictive models obtained from multivariate image analysis applied to QSAR (nematocidal: $r^2 = 0.750$ and $r^2_{pred} = 0.751$; antibacterial: $r^2 = 0.650$ and $r^2_{pred} = 0.668$) were employed to estimate the biological activities of the proposed compounds. At least two chemical candidates for each endpoint exhibited promising agrochemical performance, as the substituents $R^1 = CF_3$ or 2,4-diCl, $R^2 = CH_2CH_2Cl$ or CH_2CH_2Br, and $X = SO_2$ demonstrated a synergistic effect on the nematocidal and antibacterial activities. The promising outcomes were supported by docking studies against the acetylcholinesterase (for *M. incognita*) and β-ketoacyl-acyl carrier protein synthase (for *Xoo*) enzymes.

1. Introduction

Phytoparasitic nematodes (or roundworms) are a major cause of damages to agriculture. Thus, the development of non-phytotoxic nematicides is necessary to guarantee the conservation of various crops and, at the same time, to provide alternative chemicals for pest control and to act against resistant species. *Meloidogyne incognita* (Kofold & White) Chitwood is a main type of nematode that mostly affects sugarcane (Figueiredo et al., 2009), soybean (Barbosa et al., 2009), and coffee crops (Oliveira et al., 2009), but also others. In turn, *Xanthomonas oryzae* pv. *oryzae* (Ishiyama) Swings, van den Mooter, Vauterin, Hoste, Gillis, Mew & Kersters (*Xoo*) causes rice bacterial leaf blight, thus greatly affecting the economy worldwide (Yen, 2020).

Biopesticides have been widely used for pest control, given their advantages in terms of lower toxicity than conventional pesticides, effectiveness in small quantities, and so on. For example, biopesticides comprise ≈ 5% of the Indian pesticide market (Kumar et al., 2019). Another advantage is the selectivity, as reported elsewhere for fungi specifically against *Aedes aegypti* L. Karthi et al., (2020) and *Spodoptera litura* Fab. Karthi et al., (2019). However, chemical pesticides are advantageous in practical terms and may be designed and synthesized more easily.

Recent studies have demonstrated that some amides containing the 1,3,4-thiadiazole moiety (Fig. 1) may tackle *M. incognita* and *Xoo* simultaneously and, therefore, these compounds are promising chemical candidates for crop protection (Jixiang et al., 2019). Accordingly, chemical modification in these compounds may improve their agrochemical performance and, at the same time, provides molecular diversity useful in the case of appearance of resistance. The effect of chemical modifications on the biological response can be evaluated using computational strategies for ligand and structure-based molecular design. Quantitative structure-activity relationships (QSAR) aim to find a correlation between molecular descriptors and the corresponding biological data using a regression model (Todeschini et al., 2020). In turn, docking studies are applied to understand the mode of interaction of a molecule with the respective biological target (usually an enzyme) (Lengauer and Rarey, 1996). Together, these methods are powerful tools to predict and explain the biological activities of novel proposed compounds.

The QSAR method employed herein is based on multivariate image analysis descriptors (MIA-QSAR). Different from CoMFA and CoMSIA

* Corresponding author.
E-mail address: matheus@ufla.br (MP. Freitas).

https://doi.org/10.1016/j.napere.2022.100003
Received 18 April 2022; Received in revised form 29 April 2022; Accepted 8 May 2022

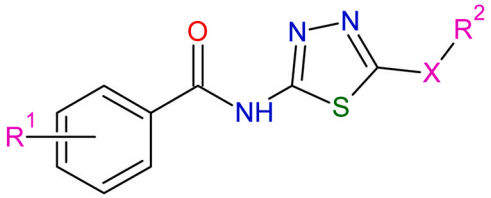

Fig. 1. *N*-(1,3,4-thiadiazol-2-yl)benzamides studied as nematocidal and antibacterial compounds. X = S or SO_2, R^1 and R^2 = substituents at the phenyl and X groups, respectively.

Table 1
Substituted *N*-(1,3,4-thiadiazol-2-yl)benzamides and the respective nematocidal (pLC_{50}, LC_{50} in mol L^{-1}) and antibacterial activities (pEC_{50}, EC_{50} in mol L^{-1}).

Compound	R^1	R^2	X	pLC_{50}	pEC_{50}
1	2-CF_3	CH_2-2-Pyr(3-Cl,5-CF_3)	S	4.328	3.801
2	2-F	CH_2-2-Pyr(3-Cl,5-CF_3)	S	4.183	3.944
3	H	CH_2-2-Pyr(3-Cl,5-CF_3)	S	3.436	3.859
4	2,4-diCl	CH_2-2-Pyr(3-Cl,5-CF_3)	S	3.899	4.149
5	2-OCH_3	CH_2-2-Pyr(3-Cl,5-CF_3)	S	3.505	4.032
6	4-F	CH_2-2-Pyr(3-Cl,5-CF_3)	S	3.920	4.124
7	2-CF_3	CH_2-Ph(4-CN)	S	2.882	3.398
8	2-CF_3	CH_2-Ph(2-F)	S	3.179	3.297
9	2-CF_3	CH_2-Ph(4-Cl)	S	3.102	3.075
10	2-CF_3	CH_3	S	3.710	3.818
11	2-CF_3	CH_2CH_3	S	3.697	3.590
12	2-CF_3	$(CH_2)_2CH_3$	S	3.575	3.556
13	2-CF_3	$(CH_2)_3CH_3$	S	3.536	3.253
14	2-CF_3	$(CH_2)_4CH_3$	S	3.497	3.904
15	2-CF_3	CH_2CN	S	3.911	3.753
16	2-CF_3	$(CH_2)_2CN$	S	3.801	3.559
17	2-CF_3	$(CH_2)_3CN$	S	3.652	3.471
18	2-CF_3	$(CH_2)_2CFCF_2$	S	3.554	3.588
19	2-CF_3	CH_2CH_2F	S	4.167	4.243
20	2-CF_3	CH_2CH_2Cl	S	4.146	4.164
21	2-CF_3	CH_2CH_2Br	S	4.015	4.174
22	2-CF_3	CH_2-Ph(4-CN)	SO_2	3.175	3.693
23	2-CF_3	CH_2-Ph(2-F)	SO_2	3.406	3.633
24	2-CF_3	CH_2-Ph(4-Cl)	SO_2	3.315	3.420
25	2-CF_3	CH_3	SO_2	4.201	4.245
26	2-CF_3	CH_2CH_3	SO_2	3.948	3.885
27	2-CF_3	$(CH_2)_2CH_3$	SO_2	3.663	3.825
28	2-CF_3	$(CH_2)_3CH_3$	SO_2	3.577	3.750
29	2-CF_3	$(CH_2)_4CH_3$	SO_2	3.385	3.734
30	2-CF_3	CH_2CN	SO_2	4.343	4.689
31	2-CF_3	$(CH_2)_2CN$	SO_2	4.046	4.605
32	2-CF_3	$(CH_2)_3CN$	SO_2	3.751	3.692
33	2-CF_3	$(CH_2)_2CFCF_2$	SO_2	4.039	3.784
34	2-CF_3	CH_2CH_2F	SO_2	4.771	5.982
35	2-CF_3	CH_2CH_2Cl	SO_2	4.721	5.488
36	2-CF_3	CH_2CH_2Br	SO_2	4.684	4.674

[a] Test set compounds randomly selected.

methods, which have been applied to model the antibacterial activities of the compounds of Fig. 1 (Jixiang et al., 2019), the MIA-QSAR scheme screens the 2D-topology of the molecules and finds the atomic contributions to the biological effect (Freitas et al., 2005). The atoms are represented as circles with sizes proportional to the respective van der Waals radii and their pixel colors are numbered to obtain a correspondence with the atomic radius and/or electronegativity (to encode steric, hydrophobic, and electrostatic effects) (Freitas et al., 2015). This

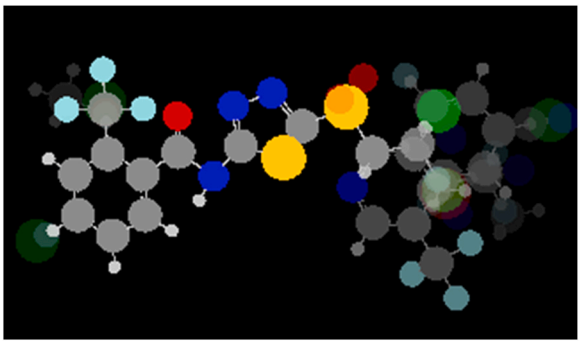

Fig. 2. Superimposed images used in the MIA-QSAR modeling demonstrating the congeneric and variable moieties in the *N*-(1,3,4-thiadiazol-2-yl)benzamides data set.

Table 2
Statistical parameters obtained from the MIA-QSAR models of the nematocidal (pLC_{50}) and antibacterial (pEC_{50}) activities.

Parameter	pLC_{50}	pEC_{50}
PLS components	4	4
RMSEc	0.238	0.359
r^2	0.750	0.650
RMSE y-rand	0.353	0.396
$r^2_{y\text{-rand}}$	0.440	0.550
$^{c}r^2_p$	0.482	0.254
RMSEcv	0.333	0.506
q^2	0.524	0.341[a]
RMSEp	0.205	0.397
r^2_{pred}	0.751	0.668
r^2_m	0.739	0.576
$\bar{r}^2_m$	0.832	0.506
Δr^2_m	0.084	0.134

[a] Increases to *ca.* 0.5 after the removal of anomalous predictions for **34** and **35**.

approach is particularly valuable in cases where the data set corresponds to a congeneric series of compounds, whose substituents explain the variance in the activities block.

2. Materials and Methods

A series of 36 *N*-(1,3,4-thiadiazol-2-yl)benzamides (Table 1) previously reported and tested against *M. incognita* and *Xoo* (Jixiang et al., 2019) was used in the MIA-QSAR modeling, and the biological data are described in terms of pLC_{50} (LC_{50} = median lethal concentration, in mol L^{-1}) and pEC_{50} (EC_{50} = concentration required to induce half of the maximum effect, in mol L^{-1}), respectively. The MIA molecular descriptors are pixel values (RGB scale) of colored bitmap images representing the molecules in the data set. Thus, the molecular descriptors vary in orientation and intensity, as the substituents change from a molecule to another. Each image was sketched using the GaussView program (Dennington et al., 2008) in such a way that the congruent substructures were perfectly superimposable, whereas the substituents explained the variance in the biological data (the ***y***-block) (Fig. 2). The atoms in molecules were represented as circles sized proportionally to the respective van der Waals radii (r_{vdW}), and the atom colors (RGB pixels ranging from 0 for black to 765 for white) were renumbered to match the corresponding r_{vdW} (MIA_{rvW} model), electronegativity (MIA_{ε} model), and r_{vdW}/ε ($MIA_{evdW/\varepsilon}$ model) values (Freitas et al., 2015). Each image of 300 × 354 pixels was unfolded to a row vector and grouped to give a 36 × (300 × 354) data matrix (**X**-matrix). The **X**-matrix was randomly split into training (75%) and

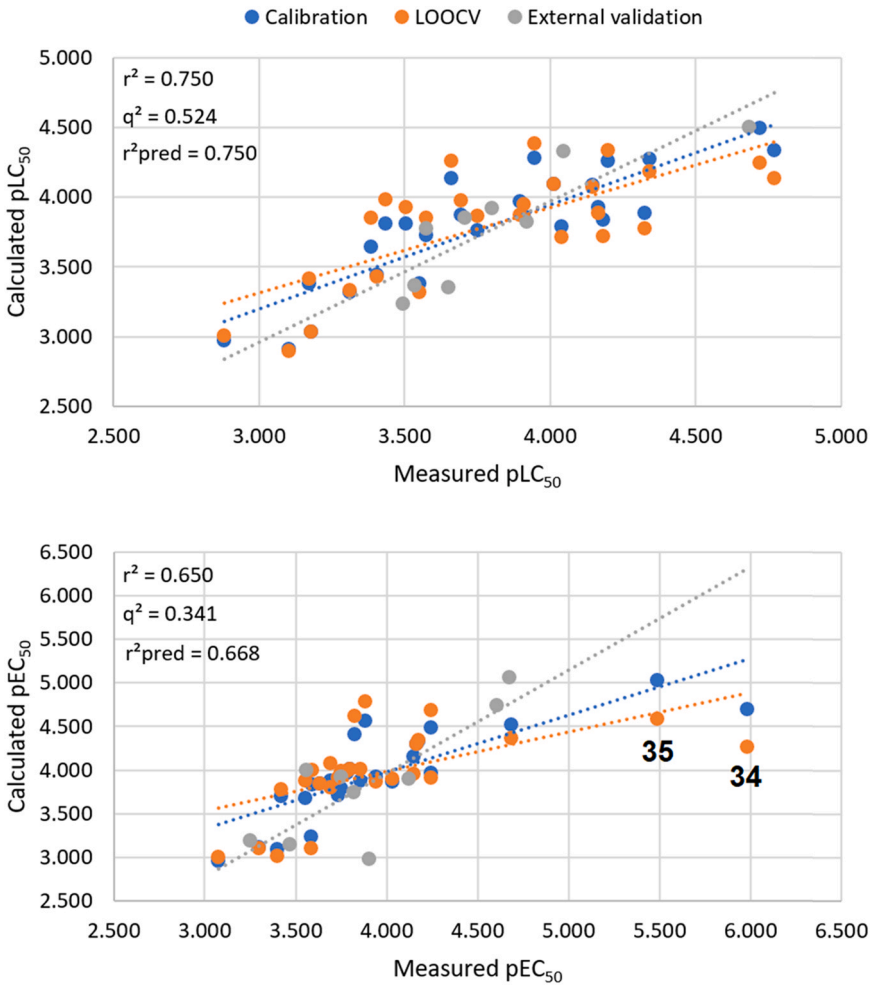

Fig. 3. Plots of experimental *vs.* calculated pLC_{50} and pEC_{50} obtained from the MIA-QSAR models.

test (25%) sets, and the former was regressed against the ***y***-block through partial least squares (PLS) regression. The regression models were both internally and externally validated, and their quality was evaluated by means of root mean square errors (RMSE) and determination coefficients in calibration (r^2), leave-one-out cross-validation (q^2), and prediction for the test set (r^2_{pred}) (Tropsha, 2010). Additional validation metrics included r^2_m (and $\hat{r}^2_m$ and Δr^2_m derivatives), which is a measure of the proximity between the observed and predicted activity (Roy et al., 2013), and ${}^{c}r^2_p$, which is a chance correlation test used to gain insight into the difference between the actual r^2 value and that obtained after scrambling the ***y***-block (Mitra et al., 2010). The influence of the molecular descriptors on the response variable was analyzed using MIA contour maps, which consist of variable importance in projection (VIP) score and PLS regression coefficient (**b**) plots. These indicate how much and how (increasing or decreasing) the substituents affect the biological activity, respectively (Barigye et al., 2016). This procedure was performed using the Chemoface program (Nunes et al., 2012).

Recent studies have shown that *Xoo* FabH can be a potential target for bactericide development, since this enzyme is critical for the survival of pathogenic bacteria (Zhao et al., 2020). β-Ketoacyl-acyl carrier protein synthase III (FabH) condenses acetyl-CoA with malonyl-ACP to initiate fatty acid biosynthesis, whereas its inhibition stops the reaction (Nanson et al., 2015). The active site of FabH consists of a catalytic triad centered around Cys/His/His residues. The only available crystal structure of *Xanthomonas oryzae pv. oryzae* FabH (*Xoo*FabH) was retrieved from the Protein Data Bank (code: 3FK5). In turn, the nematocidal activity is originated from the inhibition of acetylcholinesterase (AchE), an enzyme that ends nerve impulses by hydrolyzing acetylcholine to acetic acid and choline at the synaptic terminal and neuromuscular junction (Wei et al., 2021). To obtain structural insight into the ligand-enzyme interaction, the crystal structure of *M. incognita* AchE (*Mi*AchE) was obtained by homology modelling (Fiser, 2010). The modeling started with a systematic search in the Swiss Bioinformatics Resource Portal (Expasy) to get the primary structure of the *Mi*AchE using the UniProt database as a search tool ($author1$ et al., 2021). This profile was then used to search the PDB for known protein structures using the target sequence as the query. The primary sequence of the target protein was aligned with the template protein using the SIM similarity program (Huang and Miller, 1991). The templates were ranked based on the alignment score and the structural quality according to WHAT_CHECK (Hooft et al., 1996). The *Mi*AchE was constructed using the SWISS-MODEL server (Waterhouse et al., 2018).

A molecular docking study was carried out to validate the QSAR outcomes and to explain the binding affinity of the *N*-(1,3,4-thiadiazol-

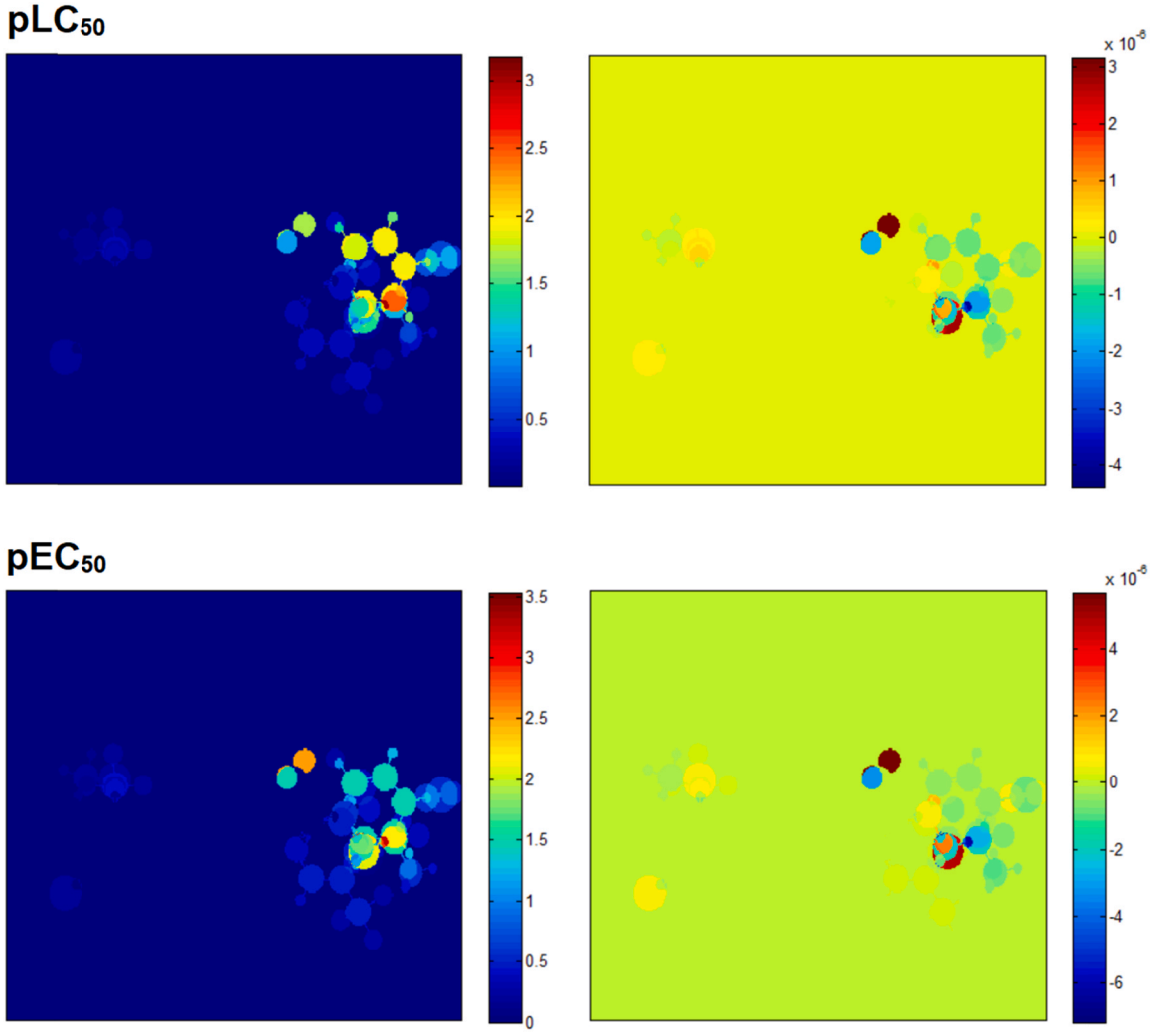

Fig. 4. MIA contour maps used to investigate how (**b**) and how much (VIP) the substituents R^1 and R^2 affect the pLC_{50} and pEC_{50} data.

2-yl)benzamides to the FabH (EC 2.3.1.41) and AchE (EC 3.1.1.7) enzymes (Rodrigues et al., 2021). The three-dimensional (3D) structures of the ligands were prepared and optimized with AMBER force field (GAFF) parameters and AM1-BCC charges. Subsequently, they were docked into the *Xoo*FabH and *Mi*AchE binding site using the Molegro Virtual Docker software (Thomsen and Christensen, 2006), a fast and flexible docking program that gives the most likely conformation of ligand binding to a macromolecule. The Moldock Score [GRID] function is a hybrid search algorithm that combines the differential evolution optimization technique with a cavity prediction algorithm during the searching procedure, which allows fast and accurate recognition of potential binding modes, the poses. It is derived from the Piecewise Linear Potential (PLP), a simplified potential whose parameters are fit to protein-ligand structures and binding data scoring functions and further extended in GEMDOCK program (Generic Evolutionary Method for molecular DOCK) with a new hydrogen bonding term and new charge schemes (Thomsen and Christensen, 2006). The grid-based scoring functions precalculated potential-energy values on an evenly spaced cubic grid to speed up calculations. The energy potential was evaluated using tri-linear interpolation between relevant grid points. A grid of 0.30 Å in resolution and 10 Å in radius from the inhibitor to the binding site was used. MolDock SE (Simplex Evolution) was used as a search algorithm, and the maximum number of poses to generate was 100. Potential binding sites were identified using the built-in cavity detection algorithm. A grid covering the protein is created and at every grid point a sphere was placed. It was checked whether this sphere overlaps with any of the spheres determined by the van der Waals radii of the protein atoms. The cavities identified by the cavity detection algorithm were then used by the guided differential evolution search algorithm to focus the search, to that specific area during the docking simulation.

3. Results and Discussion

The nematocidal activities of the compounds of Table 1 have been modeled for the first time, while the results obtained for the antibacterial were compared to a 3D-QSAR model previously reported (Jixiang et al., 2019). It is worth noticing that these bioactivities display close relationship with each other (r^2 = 0.67), which means that, in general, compounds having high nematocidal activity have also high

Table 3
Proposed molecules based on the combination of substructures of the most active compounds (in parenthesis) and the respective predicted nematocidal (pLC_{50}) and antibacterial (pEC_{50}) activities.

Proposal	R^1	R^2	X	pLC_{50}	pEC_{50}
P1 (1 +19)	2-CF_3	CH_2-2-Pyr(3-Cl,5-CF_3)	SO_2	4.643	4.596
P2 (2 +19)	2-F	CH_2-2-Pyr(3-Cl,5-CF_3)	SO_2	4.283	4.649
P3 (2 +19 / 2 +34)	2-F	CH_2CH_2F	SO_2	3.963	4.761
P4 (2 +20 / 2 +35)	2-F	CH_2CH_2Cl	SO_2	4.201	5.087
P5 (2 +21 / 2 +36)	2-F	CH_2CH_2Br	SO_2	4.234	5.115
P6 (2 +25)	2-F	CH_3	SO_2	3.955	4.508
P7 (2 +25)	2-F	CH_3	S	3.511	3.771
P8 (2 +30)	2-F	CH_2CN	SO_2	3.927	4.573
P9 (2 +30)	2-F	CH_2CN	S	3.483	3.836
P10 (2 +31)	2-F	$(CH_2)_2CN$	SO_2	3.949	4.785
P11 (2 +31)	2-F	$(CH_2)_2CN$	S	3.505	4.048
P12 (2 +33)	2-F	$(CH_2)_2CFCF_2$	SO_2	3.507	3.979
P13 (2 +33)	2-F	$(CH_2)_2CFCF_2$	S	3.063	3.242
P14 (4 +19)	2,4-diCl	CH_2CH_2F	S	3.692	4.257
P15 (4 +20)	2,4-diCl	CH_2CH_2Cl	S	3.930	4.583
P16 (4 +21)	2,4-diCl	CH_2CH_2Br	S	3.963	4.611
P17 (4 +25)	2,4-diCl	CH_3	SO_2	4.127	4.742
P18 (4 +30)	2,4-diCl	CH_2CN	SO_2	4.099	4.806
P19 (4 +31)	2,4-diCl	$(CH_2)_2CN$	SO_2	4.121	5.018
P20 (4 +34)	2,4-diCl	CH_2CH_2F	SO_2	4.136	4.994
P21 (4 +35)	2,4-diCl	CH_2CH_2Cl	SO_2	4.374	5.320
P22 (4 +36)	2,4-diCl	CH_2CH_2Br	SO_2	4.407	5.348
P23 (5 +19)	2-OCH_3	CH_2CH_2F	S	3.228	4.093
P24 (5 +20)	2-OCH_3	CH_2CH_2Cl	S	3.466	4.419
P25 (5 +21)	2-OCH_3	CH_2CH_2Br	S	3.499	4.447
P26 (5 +25)	2-OCH_3	CH_3	SO_2	3.663	4.578
P27 (5 +30)	2-OCH_3	CH_2CN	SO_2	3.635	4.642
P28 (5 +31)	2-OCH_3	$(CH_2)_2CN$	SO_2	3.657	4.854
P29 (5 +34)	2-OCH_3	CH_2CH_2F	SO_2	3.672	4.831
P30 (5 +35)	2-OCH_3	CH_2CH_2Cl	SO_2	3.910	5.156
P31 (5 +36)	2-OCH_3	CH_2CH_2Br	SO_2	3.943	5.184
P32 (6 +19)	4-F	CH_2CH_2F	S	3.421	4.044
P33 (6 +20)	4-F	CH_2CH_2Cl	S	3.659	4.370
P34 (6 +21)	4-F	CH_2CH_2Br	S	3.692	4.398
P35 (6 +25)	4-F	CH_3	SO_2	3.856	4.529
P36 (6 +30)	4-F	CH_2CN	SO_2	3.829	4.593
P37 (6 +31)	4-F	$(CH_2)_2CN$	SO_2	3.850	4.805
P38 (6 +34)	4-F	CH_2CH_2F	SO_2	3.865	4.781
P39 (6 +35)	4-F	CH_2CH_2Cl	SO_2	4.103	5.107
P40 (6 +36)	4-F	CH_2CH_2Br	SO_2	4.136	5.135

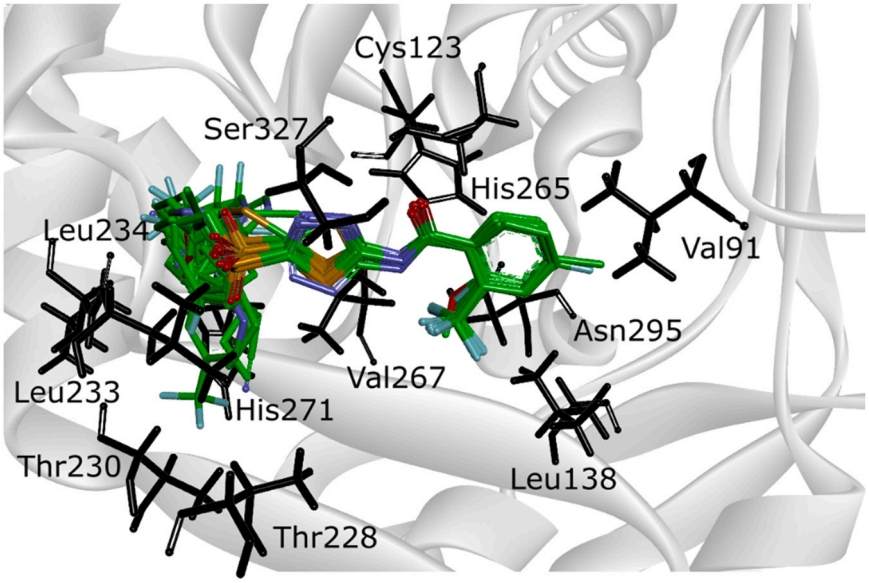

Fig. 5. Superposition of compounds **1 – 36** in the *Xoo*FabH active site.

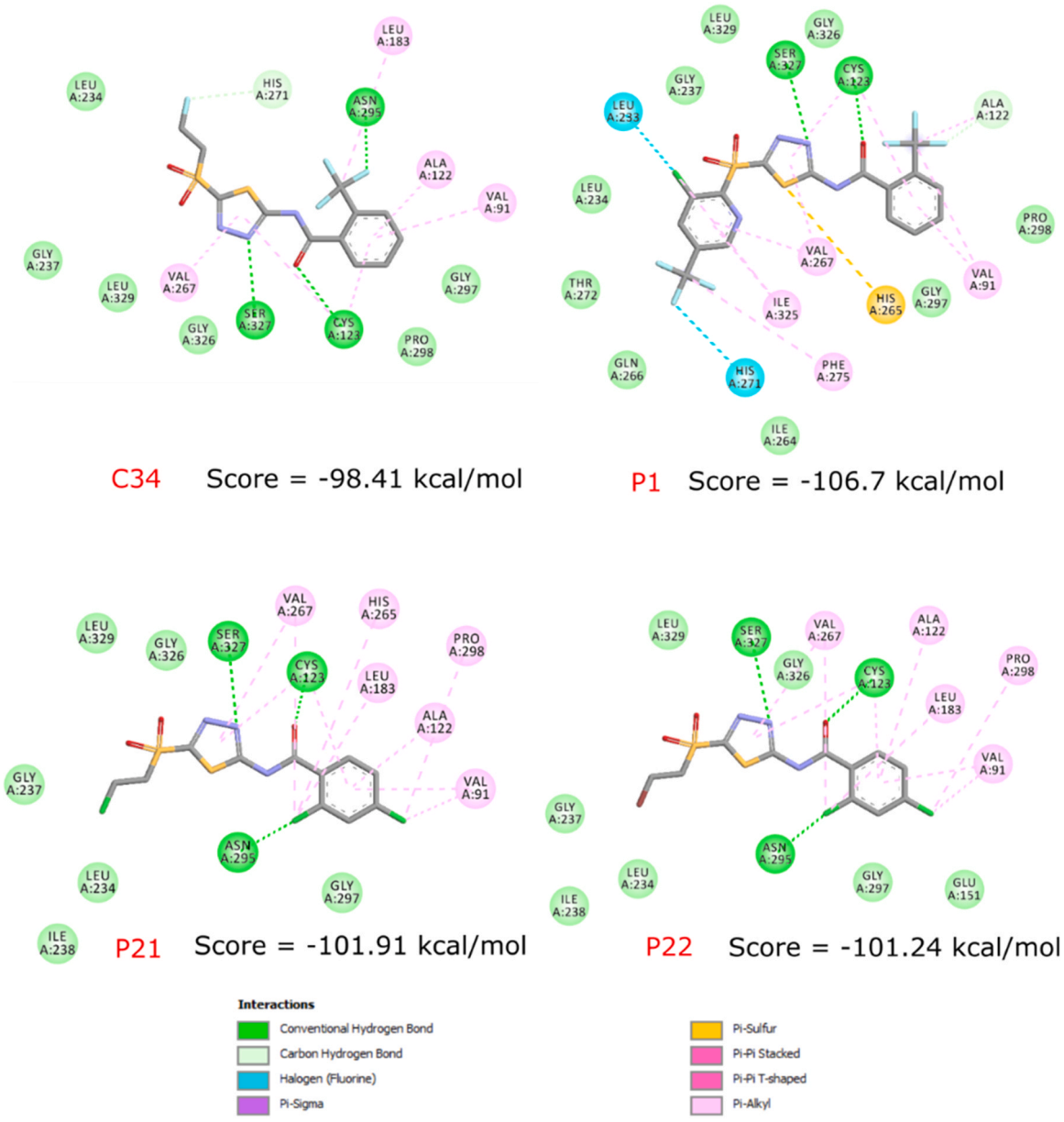

Fig. 6. Important ligand-*Xoo*FabH interactions obtained from the docking studies and the respective energy score values.

antibacterial activity. The QSAR models were generated from MIA molecular descriptors encoding r_{vdW}, ε, and the r_{vdW}/ε ratio, but only the latter presented modeling capability, demonstrating that steric and electrostatic effects together explain the variance in the biological data (pLC_{50} and pEC_{50}). Both models overcome the cut-off values required for the key parameters of calibration and validation, that is, $r^2 > 0.6$, and q^2 and $r^2_{pred} > 0.5$ (Todeschini et al., 2020), excepting for the leave-one-out cross-validation (LOOCV) of the pEC_{50} data (Table 2). However, it is clear from Fig. 3 that the calculated pEC_{50} values for compounds **34** and **35** are deleterious to the regression lines in the calibration and LOOCV, since these compounds possess the highest pEC_{50} and the regression coefficients could not precisely extrapolate these values for the samples left out. Removal of these compounds from the regression line of experimental *vs.* calculated pEC_{50} increases both r^2 and q^2.

The $^cr^2_p$ values (average of 10 cycles) were only marginally inferior to the cut-off value recommended of 0.5 in both pLC_{50} and pEC_{50} models, but $r^2_{y\text{-}rand} < r^2$ ($^cr^2_p > 0$) in all y-randomization cycles analyzed, confirming that the good performance in calibration was not obtained due to chance correlation. Moreover, considering that external validation is the only way to establish a reliable QSAR model (Golbraikh and Tropsha, 2002), the scopes of the regression lines in the prediction for the test set were analyzed and the r^2_m parameter used for this purpose was found to be acceptable, *i.e.* > 0.5 in both cases. The test samples used herein are different from those of the literature (Jixiang et al., 2019), where the selection criterion is not given, but the

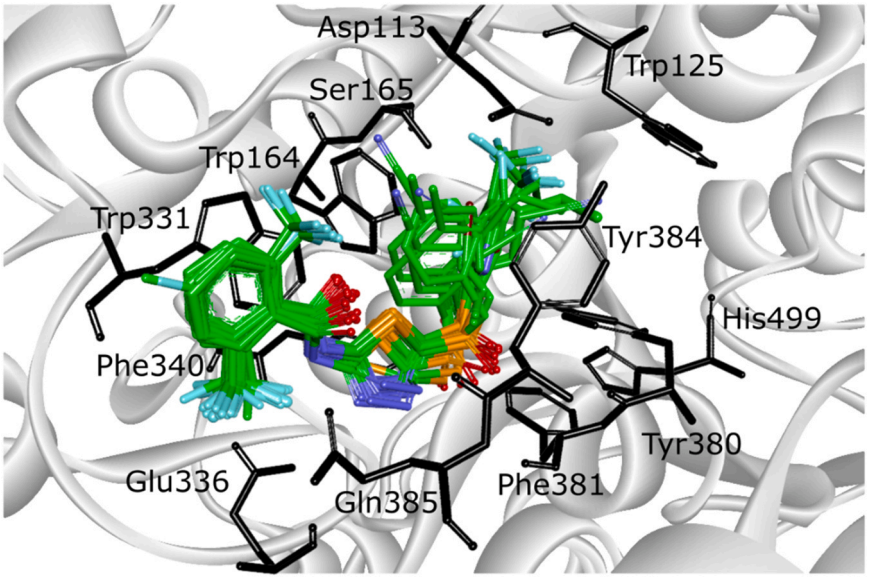

Fig. 7. Superposition of compounds **1** − **36** in the *Mi*AchE active site.

scattering plot of experimental *vs.* calculated pEC_{50} given herein is similar to that obtained from CoMFA analysis, whose main goal was to interpret the structural features in terms of molecular field analysis. Yet, our model seems to be more reliable for prediction because of a better scope of the regression line related to the predicted pEC_{50} values.

To understand how and by which extent the molecular substituents in the *N*-(1,3,4-thiadiazol-2-yl)benzamides affect the biological responses, the MIA contour maps stemming from variable importance in projection (VIP) scores and PLS regression coefficients (**b**) of Fig. 4 were analyzed. The plots for pLC_{50} and pEC_{50} are very similar, indicating that the substituents responsible for affecting the nematocidal activity are also important for antibacterial activity. From the VIP plots of both endpoints, substituents at the R^2 position appear to play a more important role than those at R^1. According to the **b**-plots, aryl and long chain alkyl groups (particularly butyl) at R^2 contribute to decrease the pLC_{50} and pEC_{50} values, while halogenated carbon chains and X = SO_2 rather than S increase these values. Therefore, unprecedented compounds were proposed based on the insights obtained from the MIA-plots and by combining the variable moieties of compounds with pLC_{50} and/or pEC_{50} higher than 4.00, giving the 40 molecules (**P1** − **P40**) of Table 3.

From the proposed compounds of Table 3, at least two nematocidal (**P1** and **P22**) and two antibacterial candidates (**P21** and **P22**) demonstrated promising performances, as the respective predicted pLC_{50} and pEC_{50} were significantly higher than 4.0 and 5.0. These values are close to the best experimental data, but it should be born in mind that **34** and **35** have anomalously high experimental pEC_{50} values, according to the QSAR model. Therefore, the proposed compounds above are worth of further development through synthesis and biological tests. To validate the QSAR findings and to understand the interaction mechanisms of the studied compounds in the biological targets, docking studies were carried out on acetylcholinesterase (AChE) (Wei et al., 2021) and β-ketoacyl-acyl carrier protein synthase III (KAS III, FabH) (Zhao et al., 2020) enzymes, which are responsible for the nematocidal and antibacterial activities, respectively.

The *Xoo*FabH active site analyzed was defined as a subset region next to Cys/His/Asn catalytic triad. The binding site on the protein was defined as extending in X, Y and Z directions around the selected cavity (693.6 $Å^3$) with a radius of 12.0 Å. To account for side chain flexibility, the amino acid residues around 6.0 Å from the center of cavity were selected to be kept flexible during the docking simulation. The docked 3D structures of compounds were scored, re-ranked, and the poses obtained were selected according to two criteria: the pose with lowest energy and the pose with similar spatial position for all compounds. It is possible to observe in Fig. 5 that the selected poses into the *Xoo*FabH active site have similar spatial coordinates. R^1 substituents are surrounded by Val91 and Asn295 residues. Compounds with a 2-CF_3 substituent can form hydrogen bonding with Asn295. Hydrogen bonding interactions are observed between the nitrogen atom of the thiadiazol ring and Ser327, and between the carbonyl group and Cys123. The nonpolar residues Leu233, Leu234, and polar residues His271, Thr228, and Thr230, posed at the site´s entrance, surround the R^2 substituents. The proposed compounds **P1**, **P21** and **P22** were docked into the *Xoo*FabH active site and Fig. 6 demonstrates the interactions with the amino acids. The score energy values obtained for these three proposed compounds in the *Xoo*FabH enzyme were higher than that for compound **34**.

The primary sequences of *M. incognita* and *Tetronarce californica* AchE were aligned and our results show a sequence identity of *ca.* 50% (Supplementary Material). This means that for very similar proteins (about 50% identical residues) the chance of completely incorrect annotation is low. The SWISS-MODEL server was used to generate the crystal structure of *Mi*AchE and the 6H14 structure from the PDB (Oukoloff et al., 2019) was used for modeling. The quality of the homology model was evaluated by different tools, such as the Ramachandran plot (Supplementary Material). The modeled protein represents 91.68% of overall residues in the most favored regions, representing a good quality model. The RMSD value of 2.64 Å was found in the best superimposition of the protein structures. The binding site is located centered around the Trp/Tyr/His residues with a cavity of 178.84 Å. All docking poses showed a conformation of the benzamide scaffold within the *Mi*AchE active site (Fig. 7), with a π-π stacking interaction with Trp331, and formation of hydrogen bond

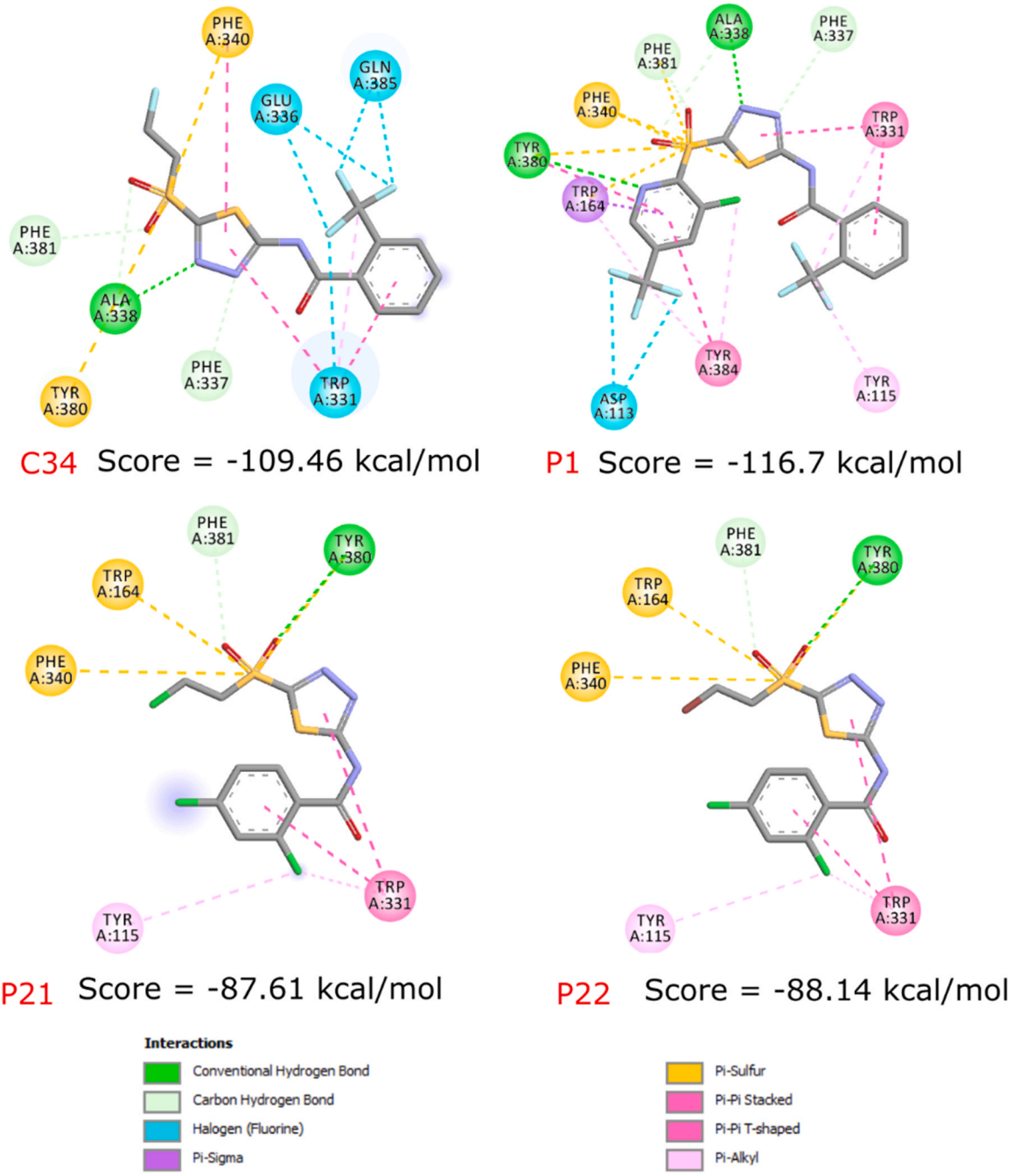

Fig. 8. Important ligand-*Mi*AchE interactions obtained from the docking studies and the respective energy score values.

between 2-CF_3 and the backbone carbonyl group of Glu336 and Gln385. Substituents at the R^2 position are surrounded by Asp113, Trp125, Trp164, Ser165, Tyr380, Phe381, Tyr384n, and His499. The proposed compounds **P1**, **P21**, and **P22** were docked into to *Mi*AchE active site and Fig. 8 demonstrates the interactions with the amino acids.

The performance of docking models is mostly measured in terms of their ability to discriminate between active and inactive compounds by calculating the docking energies. The correlations between the calculated energy score values of the studied compounds and the experimental bioactivities are shown in Fig. 9, and both plots display $R^2 \geq 0.5$. This acceptable concordance validates our QSAR studies and also indicates that *Mi*AChE and *Xoo*FabH may be biological targets for the studied compounds.

To attest our theoretical findings, the proposed compounds should be synthesized according to a similar procedure described in the literature (Jixiang et al., 2019), which is based on a three- to four-step reaction, and then assayed against *M. incognita* (by measuring the mortality rate at 50 mg L^{-1} using fosthiazate, fluopyram, and avermectin as controls) and rice bacteria *Xoo* (by measuring the

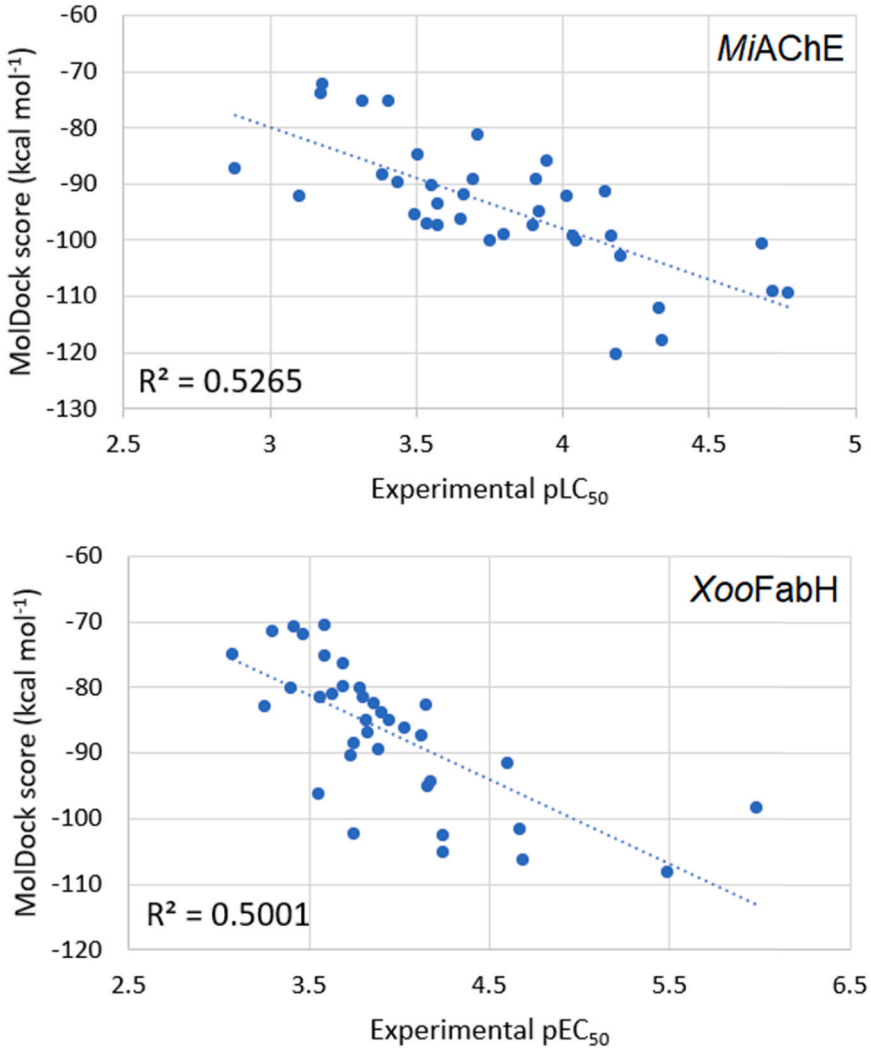

Fig. 9. Plots of experimental and calculated pLC_{50} and pEC_{50} *vs.* MolDock scores.

concentration to inhibit the activity of *Xoo* in 50% using fluopyram, bismerthiazol, and thiodiazole copper as controls).

4. Conclusion

The MIA-QSAR models built were satisfactorily predictive and indicated that specific substituents at the R^2 position, particularly those containing Cl and Br halogens, contribute to increase both the nematocidal and antibacterial effects of *N*-(1,3,4-thiadiazol-2-yl)benzamides. These outcomes were corroborated by docking studies, which showed the chemical moieties mostly affecting the interaction with the respective enzymes and, therefore, that are responsible for the biological activities. Accordingly, at least two agrochemical candidates for each endpoint were proposed for further experimental validation, whose predictions were corroborated by docking studies.

Declaration of Competing Interest

The authors declare that they have no known competing financial interests or personal relationships that could have appeared to influence the work reported in this paper.

Acknowledgements

The authors are thankful to Coordenação de Aperfeiçoamento de Pessoal de Nível Superior, Brazil (CAPES, funding code: 001), Conselho Nacional de Desenvolvimento Científico e Tecnológico, Brazil (CNPq, grant number: 306830/2021-3), and Fundação de Amparo à Pesquisa do Estado de Minas Gerais, Brazil (FAPEMIG) for financial support of this research.

Appendix A. Supporting information

Supplementary data associated with this article can be found in the online version at doi:10.1016/j.napere.2022.100003.

References

Figueiredo, A., França, R.O., Santos, M.A., 2009. Caracterização da variabilidade genética de populações do nematoide de cisto da soja coletadas na região de Jataí (GO). Nematol. Bras. 33, 212–217.

Barbosa, B.F.F., dos Santos, J.M., Soares, P.L.M., Barbosa, J.C., 2009. Avaliação comparativa da agressividade de Meloidogyne javanica e M. incognita à variedade SP 911049 de cana-de-açúcar. Nematol. Bras. 33, 243–247.

Oliveira, D.S., Oliveira, R.D.L., Silva, D.G., Silva, R.V., 2009. Falha na adaptabilidade (fitness) de Meloidogyne incognita ao cafeeiro. Nematol. Bras. 33, 207–211.

Yen, H., 2020. Rice bacterial blight. Encyclopedia Britannica. 〈https://www.britannica.com/science/rice-bacterial-blight〉.

Kumar, K.K., Ramasamy, J.S., Murali-Baskaran, K., Senthil-Nathan, S., Surendra, P.K., Arthurs, K.D.S., 2019. Microbial biopesticides for insect pest management in India: Current status and future prospects. J. Invert. Pathol. 165, 74–81. https://doi.org/10.1016/j.jip.2018.10.008

Karthi, S., Vasantha-Srinivasan, P., Ganesan, R., Ramasamy, V., Senthil-Nathan, S., Khater, H.F., Radhakrishnan, N., Amala, K., Kim, T.-J., El-Sheikh, M.A., Krutmuang, P., 2020. Target activity of *Isaria tenuipes* (Hypocreales: Clavicipitaceae) fungal strains against dengue vector *Aedes aegypti* (Linn.) and its non-target activity against aquatic predators. J. Fungi 6, 196.

Karthi, S., Senthil-Nathan, S., Kalaivani, K., Vasantha-Srinivasan, P., Chellappandian, M., Thanigaivel, A., Ponsankar, A., Sivanesh, H., Stanley-Raja, V., Chanthini, K.M.-P., Shyam-Sundar, N., 2019. Comparative efficacy of two mycotoxins against Spodoptera litura Fab. And their non-target activity against Eudrilus eugeniae Kinb. Ecotoxicol. Environ. Saf. 183, 109474.

Jixiang, C., Chongfen, Y., Shaobo, W., Sikai, W., Shaoyuan, L., Deyu, H., Baoan, S., 2019. Novel amide derivatives containing 1,3,4-thiadiazole moiety: Design, synthesis, nematocidal and antibacterial activities. Bioorg. Med. Chem. Lett. 29, 1203–1210. https://doi.org/10.1016/j.bmcl.2019.03.017

Todeschini, R., Consonni, V., Ballabio, D., Grisoni, F., 2020. Chemometrics for QSAR Modeling. In: Brown, S.D., Tauler, R., Walczak, B. (Eds.), Comprehensive Chemometrics. Elsevier, Amsterdam.

Lengauer, T., Rarey, M., 1996. Computational methods for biomolecular docking. Curr. Opin. Struct. Biol. 6, 402–406. https://doi.org/10.1016/s0959-440x(96)80061-3

Freitas, M.P., Brown, S.D., Martins, J.A., 2005. MIA-QSAR: A simple 2D image-based approach for quantitative structure-activity relationship analysis. J. Mol. Struct. 738, 149–154. https://doi.org/10.1016/j.molstruc.2004.11.065

Freitas, M.R., Barigye, S.J., Freitas, M.P., 2015. Coloured chemical image-based models for the prediction of soil sorption of herbicides. RSC Adv. 5, 7547–7553. https://doi.org/10.1039/C4RA12070A

R.D. Dennington, T.A. Keith, M.J. Millam, GaussView 5.0, Wallingford, CT, 2008.

Tropsha, A., 2010. Best practices for QSAR model development, validation, and exploitation. Mol. Inf. 29, 476–488. https://doi.org/10.1002/minf.201000061

Roy, K., Chakraborty, P., Mitra, I., Ojha, P.K., Kar, S., Das, R.N., 2013. Some case studies on application of "r_m^{2}" metrics for judging quality of quantitative structure–activity relationship predictions: Emphasis on scaling of response data. J. Comput. Chem. 34, 1071–1082. https://doi.org/10.1002/jcc.23231

Mitra, I., Saha, A., Roy, K., 2010. Exploring quantitative structure–activity relationship studies of antioxidant phenolic compounds obtained from traditional Chinese medicinal plants. Mol. Simul. 36, 1067–1079. https://doi.org/10.1080/08927022.2010.503326

Barigye, S.J., Duarte, M.H., Nunes, C.A., Freitas, M.P., 2016. MIA-plot: a graphical tool for viewing descriptor contributions in MIA-QSAR. RSC Adv 6, 49604–49612. https://doi.org/10.1039/C6RA09593C

Nunes, C.A., Freitas, M.P., Pinheiro, A.C.M., Bastos, S.C., 2012. Chemoface: a novel free user-friendly interface for chemometrics. J. Braz. Chem. Soc. 23, 2003–2010. https://doi.org/10.1590/S0103-50532012005000073

Zhao, S., Xiao, C., Wang, J., Tian, K., Ji, W., Yang, T., Khan, B., Qian, G., Yan, W., Ye, Y., 2020. Discovery of natural FabH inhibitors using an immobilized enzyme column and their antibacterial activity against Xanthomonas oryzae pv. oryzae. J. Agric. Food Chem. 68, 14204–14211. https://doi.org/10.1021/acs.jafc.0c06363

Nanson, J.D., Himiari, Z., Swarbrick, C.M.D., Forwood, J.K., 2015. Structural characterisation of the beta-ketoacyl-acyl carrier protein synthases, FabF and FabH, of Yersinia pestis. Sci. Rep. 5, 14797. https://doi.org/10.1038/srep14797

Wei, C., Huang, J., Luo, Y., Wang, S., Wu, S., Xing, Z., Chen, J., 2021. Novel amide derivatives containing an imidazo[1,2-α]pyridine moiety: Design, synthesis as potential nematicidal and antibacterial agents. Pest. Biochem. Physiol. 175, 104857. https://doi.org/10.1016/j.pestbp.2021.104857

Fiser, A., 2010. Template-based protein structure modeling. In: Fenyö, D. (Ed.), Computational Biology: Methods in Molecular Biology (Methods and Protocols). Humana Press, Totowa.

The UniProt Consortium, UniProt: The universal protein knowledge base in 2021, Nucleic Acids Res. 49 (2021) D480–D489, doi: ⟨10.1093/nar/gkaa1100⟩.

Huang, X., Miller, W., 1991. A time-efficient, linear-space local similarity algorithm. Adv. Appl. Math. 12, 337–357. https://doi.org/10.1016/0196-8858(91)90017-D

Hooft, R.W.W., Vriend, G., Sander, C., Abola, E.E., 1996. Errors in protein structures. Nature 381, 272. https://doi.org/10.1038/381272a0

Waterhouse, A., Bertoni, M., Bienert, S., Studer, G., Tauriello, G., Gumienny, R., Heer, F.T., de Beer, T.A.P., Rempfer, C., Bordoli, L., Lepore, R., Schwede, T., 2018. SWISS-MODEL: Homology modelling of protein structures and complexes. Nucleic Acids Res. 46, W296–W303. https://doi.org/10.1093/nar/gky427

Rodrigues, N.E., de Faria, A.C., Pereira, I.V., da Cunha, E.F.F., Freitas, M.P., 2021. QSAR-Guided proposition of N-(4-methanesulfonyl)benzoyl-N′-(pyrimidin-2-yl)thioureas as effective and safer herbicides. Bull. Environ. Contam. Toxicol. https://doi.org/10.1007/s00128-022-03467-w

Thomsen, R., Christensen, M.H., 2006. MolDock: A new technique for high-accuracy molecular docking. J. Med. Chem. 49, 3315–3321. https://doi.org/10.1021/jm051197e

Golbraikh, A., Tropsha, A., 2002. Beware of q^{2}!. J. Mol. Graph. Model. 20, 269–276. https://doi.org/10.1016/S1093-3263(01)00123-1

Oukoloff, K., Coquelle, N., Bartolini, M., Naldi, M., Le Guevel, R., Bach, S., Josselin, B., Ruchaud, S., Catto, M., Pisani, L., Denora, N., Iacobazzi, R.M., Silman, I., Sussman, J.L., Buron, F., Colletier, J.-P., Jean, L., Routier, S., Renard, P.-Y., 2019. Design, biological evaluation and X-ray crystallography of nanomolar multifunctional ligands targeting simultaneously acetylcholinesterase and glycogen synthase kinase-3. Eur. J. Med. Chem. 168, 58–77. https://doi.org/10.1016/j.ejmech.2018.12.063